A comparative study of a direct and pulse electrodeposition method of TiO_2 films and its effect on photoelectrocatalytic degradation of methyl orange dye

Khadidja Hadj Larbi[1], Farid Habelhames[1], Meriem Lakhdari[1], Farid Bennabi[2], Belkacem Nessark[1], Mehdi Adjdir[3], Abdelkader Echchergui Nebatti[4], and Bouhalouane Amrani[5]*

1. *Laboratoire d'électrochimie et matériaux (LEM), Faculté de Technologie, Département de génie des procédés, Université Ferhat Abbas Sétif-1, Sétif 19000, Algérie*
2. *Laboratory of Applied Chemistry, University of Ain-Temouchent Belhadj Bouchaib, Algeria*
3. *Laboratory of Applied Organic Synthesis, Faculty of Exact and Applied Sciences, University Oran1 Ahmed Ben Bella, BP 1524 El M'Naouer, Oran 31000, Algeria*
4. *Laboratory of Materials Sciences and Applications (LMSA), University of Ain-Temouchent Belhadj Bouchaib, Algeria*
5. *Electron Microscopy Center, Faculty of Exact and Applied Sciences, University of Oran1 Ahmed Ben Bella, Oran, Algeria*

(Received 1 December 2020; Revised 21 January 2021)

The present study reports the titanium dioxide (TiO_2) films synthesized from $TiCl_3$ precursor on ITO glass substrates using two electrochemical techniques, namely direct electro-deposition (DE) and pulse electro-deposition (PE). The synthesis potential during the time-on (T_{on}) period was fixed at −1.5 V. However, the open-circuit potential was applied during the time-off (T_{off}) period. The effect of the technique of electro-deposition and T_{off} duration on the properties of TiO_2 films and their photoelectron-catalytic activity were investigated. The obtained films were investigated by X-ray diffraction (XRD), scanning electron microscopy (SEM), UV-VIS spectrometer, and photocurrent measurement respectively. It is found that the use of the PE technique at different T_{off} improves the properties of TiO_2 films compared to the DE technique. The XRD patterns show the anatase phase with a marked preferential orientation along the (101) direction for all samples. From the SEM analysis, it is seen a significant change from big multigrain agglomerates at DE to a dense film structure and small multigrain agglomerates at different T_{off}. As the T_{off} decreases from 3 s to 1 s, the photocurrent response rises and reaches a high value of about 12 mA/cm^2. Compared with DE, and under UV light the photocatalytic property of TiO_2 film synthesis via PE has been improved in the degradation of methyl orange (MO). Finally, the films deposited at low T_{off} (T_{off} =1 s) show a faster degradation of MO.

Document code: A **Article ID:** 1673-1905(2021)06-0334-8
DOI https://doi.org/10.1007/s11801-021-0193-4

Titanium dioxide (TiO_2) belongs to IV-VI semiconductor material with a wide band gap of 3.2 eV at room temperature[1]. It is well known that the TiO_2 naturally has existed in three crystalline phases such as brookite, rutile, and anatase. However, rutile and anatase crystalline phases are usually interesting in the research community due to abundant raw materials, non-toxic features, and its diverse technology applications, ie., solar cell[2], light emitting diodes[3], flat panel displays[4], gas sensors[5], temperature sensor[6]. It is obvious that non-biodegradable organic dyes endanger aquatic life and disturb the water ecosystem. Thus, the challenge to find out adequate techniques and materials to destroy undesirable organic compounds in the aqueous phase and to remove traces of organic species that are stable and difficult to oxidize by means of conventional water treatment methods[7-9]. Firstly, the most well known techniques to solve the mentioned problem are catalytic wet oxidation biodegradation and adsorption. Among these, photocatalytic degradation is preferable, which has the advantages of being a low cost and groundbreaking method to completely remove dangerous organic wastes[10]. Secondly, TiO_2 is an excellent photocatalytic material that can find applications in various fields including water splitting, environmental purification, self-cleaning, and super hydrophilic surfaces[11,12]. Owing to its simple chemical

* E-mail: amrani.bouhalouane@univ-oran1.dz

composition, its nontoxicity, chemical and biological stability, low cost and good optical transparency and its outstanding photocatalytic performance[13-15]. TiO_2 films have been deposited by various techniques, such as DC-sputtering[16] chemical spray pyrolysis[17-19], sol-gel method[6] and pulsed laser deposition[20]. Especially the electrochemical methods (direct electro-deposition (DE) and pulse electro-deposition (PE)) are interesting for some reasons, which are good reproducibility, large and non-uniform substrates can be easily coated, controllability, reliability and versatile method for the preparation of high quality films with high deposition rates see the respective handbooks for a description of electro-deposition[21,22]. Therefore, it was used in the present study.

We aimed at developing TiO_2 films on indium tin oxide (ITO) substrate using the both above mentioned methods and indicate the influence of the electro-deposition T_{off} up on the structural, morphological, optical, and photoelectron-chemical proprieties. Additionally, the obtained films were tested for the photoelectron-catalytic degradation of methyl orange (MO), where MO is a representative organic dye used extensively in the textile, printing, and photographic industries.

Based on our knowledge, it should be mentioned that no previous study was done on the synthesis of TiO_2 from $TiCl_3$ precursor using a similar synthesis process for photoelectron-catalytic degradation of MO.

The materials used were de-ionized water, ethanol (C_2H_5OH), acetone (C_3H_6O) (Analytical grade, VWR Prolabor), titanium (III) chloride $TiCl_3$ (Merck), potassium nitrate (KNO_3>98%, Aldrich), pH meter, the electro-deposition system and ITO substrates (1 cm^2 area).

The electrochemical methods with DE and PE were used to synthesis TiO_2 films. The substrates used in this work have ITO with 1 cm^2 area. Prior to each deposition, experimental substrates were cleaned carefully for a few minutes with ethanol, acetone, and de-ionized water, respectively[23]. The preparation relies on the DE and PE electro-deposition process. The methods are based on the use of conventional three electrodes cell, the set-up which is described in detail elsewhere[24,25] ITO substrates, platinum mesh and saturated calomel electrode (SCE) which were used as the working the counter and the reference electrode, respectively.

In the present case, the electrodeposition bath was a 0.25 M ($TiCl_3$)·0.5 M (KNO_3) at pH of 2.5. The deposition was carried out under potentio-static conditions with the potential range between −0.4 V and −1.8 V. The TiO_2/ITO films were prepared by applying a constant cathodic potential of −1.5 V versus SCE during 900 s, inside the bath. Subsequently, the electrodeposited films were rinsed with deionized water, and annealed at 450 °C for 4 h, with 5 °C/min heating rate. A Voltalab PGZ 301 made up of a potentiostat-galvanostat was used to perform the electrodeposition.

Various techniques were used to characterize the TiO_2 films. The phase structure of the films was investigated by X-ray diffraction (XRD) (model- Bruker D8 advance) using Cu radiation (λ=1.540 6 Å). For all measurements, the angle of incidence was kept at 2°, in order to be sensitive to the near surface regions. The film morphology was analyzed using a high resolution scanning electron microscope under 10.00 kV operating voltage. The films morphology of the obtained films was characterized using a scanning electron microscope (SEM, JSM-7600F, JEOL) under 10.00 kV operating voltage. Furthermore, the transmittance spectra were obtained using an ultraviolet-visible spectrophotometer (UV-VIS, Shimadzu 10S) measured at room temperature in the wavelength range of 200—850 nm with a scan step of 500 nm/min.

Photoactivity was studied by forming a photoelectrochemical cell with TiO_2 as a photoelectrode and platinum spiral wire as a counter electrode. The electrolytes used were 0.1 M (K_2SO_4) using a monochromatic UV-lamp source at λ=365 nm. The MO electrochemical degradation was studied with the 1 cm^2 area TiO_2/ITO sample as a working electrode. A platinum wire and SCE were used as counter electrode and a reference electrode, respectively. A single compartment electrochemical quartz cell was employed in a typical three-electrode arrangement. Electrochemical oxidation (EC) was performed using a Voltalab PGZ 301 made up of a potentiostat-galvanostat under +1.5 V-potential. MO decomposition was determined by measuring the an UV-visible absorbance at regular time intervals[26]. Initial MO concentration was 0.001 5 g/L (100 mL) in 0.1 M NaOH. UV-lamp (λ=365 nm) was positioned in front of the quartz electrochemical cells. After photoelectrocatalysis, MO concentration was determined immediately by measuring the absorbance of 2.0 mL of the MO solution using a Cary 1e UV-visible spectrophotometer. MO concentration was tested at predetermined time intervals of 10 min, 20 min, 30 min, 60 min, 120 min, 180 min, 240 min, 300 min, and 360 min.

The chronoamperometry curves obtained during TiO_2 electrodeposition and pulsed electrodeposition on ITO-coated glass substrates are shown in Fig.1.

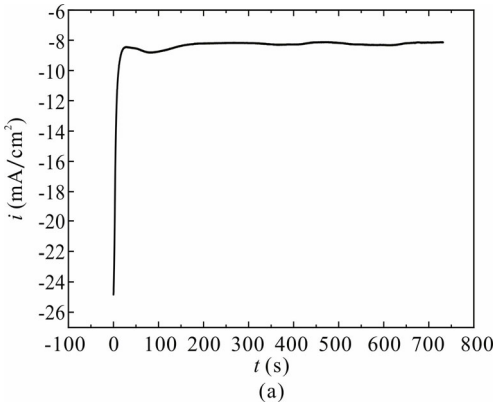

(a)

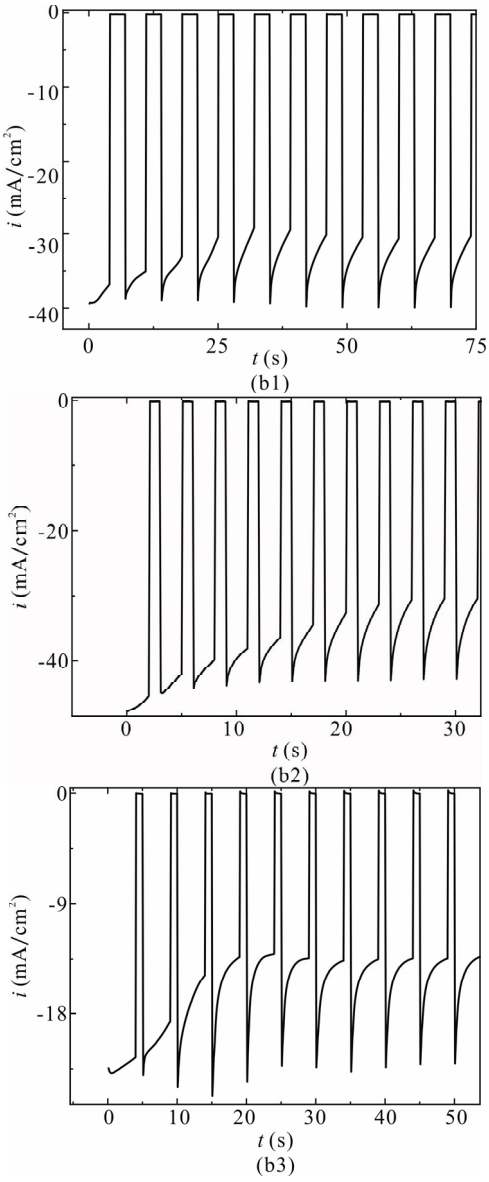

Fig.1 Curves of the TiO_2 films in 0.5 M (KNO_3) solutions at 450 °C: (a) DE (chronoamperometry) for 900 s and PE of TiO_2 thin-films for the first ten cycles with T_{on}=4 s: (b1) T_{off}=3 s; (b2) T_{off} =2 s; (b3) T_{off} =1 s

In the conventional DE plating, there is only one variable parameter, namely current density (I)[27]. The *i-t* curve of DE shows that the initial current increases rapidly at a very short time, at the beginning of the deposition process and eventually levels off results from the depletion of $TiOH_2^+$ intermediate in the pores due to the continuous growth of TiO_2 deposits. During the continuous deposition, the polymeric titanium hydroxide particles deposited at the entrance to the pore channels may continue to form large particles that may block the penetration of electrolyte into the pores of the TiO_2 thick film[28]. In PE, there are three independent variables: T_{on}, T_{off} and peak current (I_P). T_{on} is the time period when the pulses are imposed[27,29], during where −1.5 V versus SCE deposition potential is applied, and T_{off} is the relaxation time, during which open-circuit potential (OCP=+0.96 V versus SCE) is applied. The pulse pause T_{off} was varied values of 3 s, 2 s and 1 s, and the pulse T_{on} was kept constant at 4 s, respectively at room temperature, for all experiments as shown in Fig.1. In PE mode, the duty cycle (γ) corresponds to the percentage of total time of a cycle and is given by[27]

$$\gamma = \frac{T_{on}}{T_{on} + T_{off}} . \quad (1)$$

Based on the results above, a possible mechanism for the electrochemical deposition is proposed. As is rationalized above, the reduction of NO_3^- ion is essential at the initiation step of the electrodeposition:

$$NO_3^- + H_2O + 2e^- \rightarrow NO_2^- + 2OH^-, \quad (2)$$

$$Ti^{3+} + H_2O \rightarrow TiOH_2^+ + H^+. \quad (3)$$

Similarly, $TiOH_2^+$ ions in the hydrolyzed $TiCl_3$ solution react with OH^- yield polymeric Ti (III) hydroxide gel

$$TiOH^{2+} + 2OH^- \rightarrow Ti(OH)_3 . \quad (4)$$

The hydroxide gels are finally converted to TiO_2 upon annealing in the air[30,31]. In direct deposition conditions, the rate of OH^- ion formation remains constant during the process. Consequently, the DE mode allows a better control of the precipitation process. However, the PE mode is superior to fixed current deposition in terms of minimizing OH^- ion accumulation at the ITO surface, which could suffer a chemical attack at higher pH. OH^- ions formed on the cathode surface during time-on are consumed in the chemical reaction during time-off periods.

The XRD measurement of θ-2θ scan was performed on TiO_2 films on ITO substrate as shown in Fig.2 as a function of the mode of DE and PE with different time-off pulses of 3 s, 2 s and 1 s at fixed time-on of 4 s. It can be seen that all films are polycrystalline in behaviour. As indexed in Fig.2, eight diffraction patterns were observed with a different intensity peak at 2θ=25.04°, 36.99°, 37.32°, 48.70°, 53.87°, 61.67°, 68.26° and 73.74° corresponding to (101), (103), (004), (200), (105), (213), (116) and (107) planes, respectively. These last values are in good agreement with the standard diffraction data of anatase phase (JCPDS card, N° 21-1272). Besides, the preferred orientation was (101) for all films. The diffraction peaks marked by the sign of (*) correspond to ITO substrate. It is obviously seen in that case, no relative peaks of brookite or rutile phases are observed. Furthermore, the diffraction patterns of the film prepared with PE method indicate a strong intensity peak at 2θ=25.04° for the plane (101) compared to the film obtained by DE. The average crystallite size D has been estimated from XRD data using *FWHM* of the preferential peak (101) of the films prepared via both methods (DE and PE) according to Scherrer's formula[32]

$$D_{Scherrer} = 0.94\lambda/(\beta\cos\theta) , \quad (5)$$

where λ is the wavelength of X-ray radiation, θ is the Bragg diffraction angle and β is the *FWHM* of the

preferential peak of diffraction. The Scherrer method assumes that the line broadening is merely due to the contribution of small crystallite size. After calculation, the crystallites size increases from 8.48 nm for T_{off}=3 s to 9.86 nm for T_{off}=2 s until reach the max value about 10.71 nm for T_{off} =1 s. It can be seen that for T_{off} duration of 3 s, 2 s and 1 s, D may change significantly. The increase of the crystallite size with decreasing of T_{off} duration is likely due to the increase of the nucleating centres which could be caused by the drag forces exerted on the boundary motion and crystallite[33,34]. On the other hand, we found that the crystallite size of the TiO_2 films prepared by DE is bigger (11.58 nm) than the crystallite size of thin films deposited by PE. The observed increase in crystallite size could be attributed to the increasing of imperfections which enhances grain boundary mobility and growth rate[34].

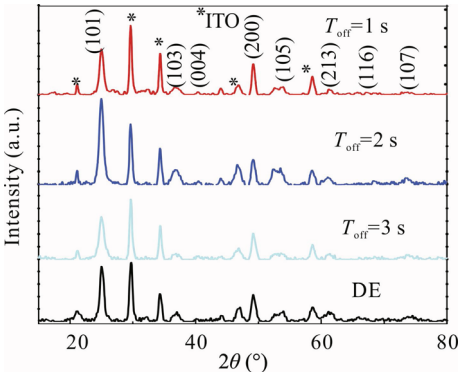

Fig.2 XRD patterns of the TiO_2 films in 0.5 M (KNO_3) solutions at 450 °C for DE and PE at different T_{off}

In order to show the influence of the synthesis methods (DE and PE) and time-off on the surface morphology, a set of samples was analyzed by the SEM technique. Fig.3 shows the typical top-view SEM images of TiO_2 films synthesized by both above-cited methods and at three time-off periods. First of all, it's clear from Fig.3 that all obtained films are relatively homogeneous and distributed almost uniform on the ITO substrate surface. However, a remarkable topography change between the two methods was observed. As seen in Fig.3 (A-A'), well defined multigrain agglomerates with an irregular big shape and large pores with a grain size of around 800 nm, which is in agreement with the XRD data. Whereas, multigrain agglomerates with regular, small shape and small pores with grain size between (110—280 nm) were obtained by the PE method. Furthermore, TiO_2 film synthesis at 3 s T_{off} consists of small nanosheets of grain size around 0.017 μm and big pores spread uniformly on the substrate surface, as shown in Fig.3(B_1). As T_{off} decreased to 2 s, the bigger nanosheets of 0.022 μm and small pores were observed (see Fig.3(B_2)). At lower T_{off} duration (1 s), the formation of dense films can be observed (see Fig.3(B_3)).

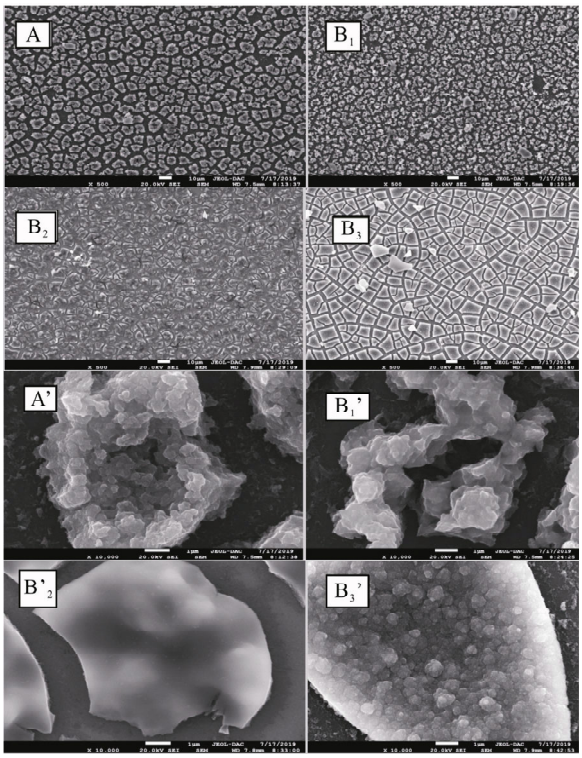

Fig.3 SEM images of patterns of the TiO_2 films in 0.5 M (KNO_3) solutions at 450 °C for DE(A-A') and PE at different T_{off}: 3 s (B_1-B_1'); 2 s (B_2-B_2'); 1 s (B_3-B_3') at low magnification (A, B_1, B_2, B_3) and high magnification (A', B_1', B_2', B_3')

The optical transmittance spectra of TiO_2 film for both electrodeposition methods synthesized by DE and PE at different time-off recorded in the wavelength region of 300—900 nm are illustrated in Fig.4. Noticeably, all deposited films present a medium transparency ranging from 40% to 67%. However, the films transmittance seems to be affected by the synthesis methods (DE and PE) and time-off duration. As seen in Fig.4, the optical transmissions of the films obtained by DE method show low value of transmittance about 42% compared to the films obtained by PE, which it reaches high value around 76%. Besides, it can be clearly seen that the average transmittance increases up to 76% with decreasing time-off duration. The increase in film transparency may be due to the improvement of crystal quality, which leads to lowering the light diffusion by the large grains size forming the film. These results are supported by XRD and MEB data. As mentioned above, the optical transmittance increases in the visible range, and the transmission edge is blue shifted also termed as Burstein-Moss shift[35,36].

This result depicts that the optical band gap (E_g) of the films was influenced by the synthesis mode and time-off duration. The band gap energy (E_g) with direct allowed transition can be determined using the Tauc relationship given by the following expression in Eq.(6)[37]

$$\alpha = \frac{A}{h\nu}(h\nu - E_g)^n, \tag{6}$$

where A is a proportionality constant, hv is the photon energy, α is the absorption coefficient, and E_g is the band gap and n=1/2 for direct or n=2 for indirect optical transitions[38]. The photon energy at the point where α^2=0 is E_g and is obtained by the extrapolation method. Based on Fig.5, it was noted that the optical band gap of TiO_2 films developed using DE and PE mode lies between 3.01 eV and 3.28 eV depending on two parameters, such as mode of the synthesis and time off duration. The lowest value of the E_g is around 3.01 eV obtained by DE mode, may be due to large grain size of this film. In addition, the E_g value increases from 3.06 eV to 3.28 eV in accordance with the decrease of T_{off} duration from 3 s to 1 s. TiO_2 prepared by PE mode could improve the specific surface area, improving the film morphology and optical properties. So, PE mode is beneficial for electro-optical materials.

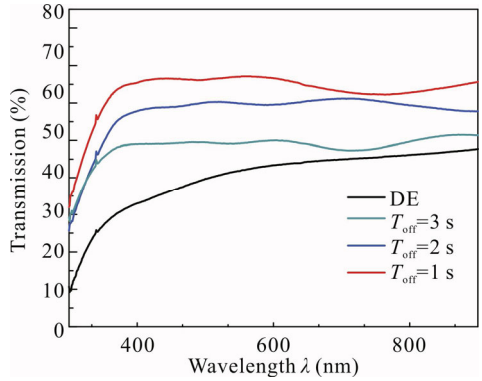

Fig.4 Optical transmittance spectra of the TiO_2 films in 0.5 M (KNO_3) solutions at 450 °C for DE and PE at different T_{off}

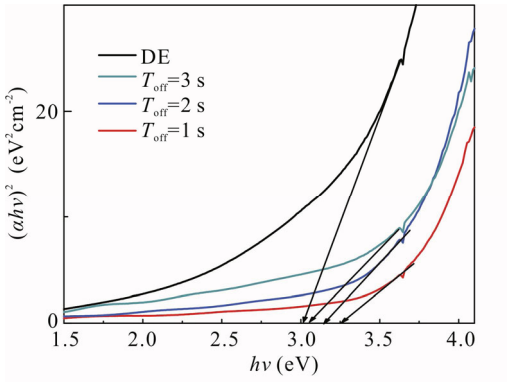

Fig.5 The band-gap estimation of the TiO_2 films in 0.5 M (KNO_3) solutions at 450 °C for DE and PE at different T_{off}

The photoelectrochemical cell is a photocurrent-generated device composed of an electrolyte, a photoactive semiconductor electrode[39]. In the present case, TiO_2 films were used as a working electrode in a photoelectrochemical cell containing potassium sulfate (K_2SO_4) 0.1 M as electrolyte solution. Fig.6 displays the photocurrent response of TiO_2 films synthesis via two modes of DE and PE at three T_{off} durations of 3 s, 2 s, and 1 s. As seen in Fig.6, a rapid generation of photocurrent response is observed when the TiO_2 film is illuminated under UV light. In both modes, TiO_2 films show anodic (positive) current under UV light. It is well known that n-type semiconductors produce an anodic photocurrent in which holes are transferred toward the electrolyte, while p-type semiconductors generate a cathodic photocurrent by transmitting electrons toward the electrolyte. Consequently, TiO_2 films have n-type conductivity[36,37,39]. Typical photocurrent-time curves are given upon switching the light on and off, with an applied potential of +0.8 V versus SCE. In the dark, there is negligible anodic photocurrent; however, under illumination of the TiO_2 surface, we observe an important anodic photocurrent. This suggests that the excited minority carriers diffuse to the surface to participate into the electrochemical reaction at the electrode interface[40]. The photocurrent detected in PE films is i=4.24 μA/cm^{-2}, i=9.11 μA/cm^{-2}, i=12.59 μA/cm^{-2} at 3 s, 2 s, and 1 s, respectively. It is clear that the photocurrent increased dramatically with decreasing the time-off value. This behavior can be explained by more efficient electron-hole pair separation. However, the photocurrent for DE films is about i=1.12 μA/cm^{-2}, which is less than PE films. This finding may be due the morphologies of the TiO_2 (see Fig.3) suggest a greater surface |electrolyte interface area which is where minority (hole) carrier collection occurs. It is therefore feasible that a greater fraction of electron-hole pair generation occurs in regions whose distance is smaller than the minority carrier diffusion length resulting in higher internal quantum efficiencies and hence greater photocurrent densities[41]. That will also be confirmed by the morphological development of TiO_2 in the PE mode.

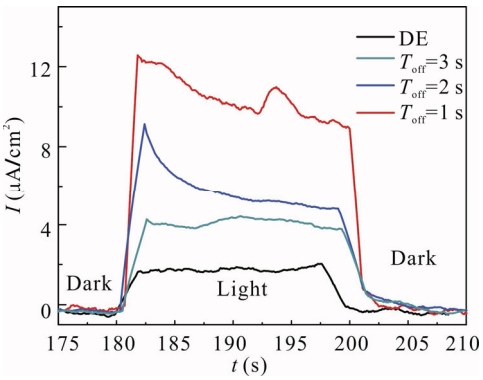

Fig.6 Photocurrent responses of the TiO_2 films in 0.5 M (KNO_3) solutions at 450 °C for DE and PE at different T_{off}

As is known, the photocatalytic process involves the activation of a TiO_2 film by natural or artificial light. As reported in the introduction section TiO_2 is semiconductor, which is characterized by valence bands

(VB) and conduction bands (CB), the region between the valence band and the conduction band is called band gap (E_g)[42]. When a TiO_2 film is illuminated with energy greater than the energy of band gap, leads to the formation of a positive hole h^+ in the VB and an electron e^- in the CB. The photogenerated e^- can react with MO dye and acceptor electrons, as oxygen molecules adsorbed on the surface of the TiO_2 or dissolved in the water, generating superoxide anions ($O_2^{\bullet-}$)[43]. The positive hole (h^+) oxidizes either pollutant directly or water to produce hydroxyl radical $HO^{\bullet}$[44]. Whereas the electron in the conduction band reduces the oxygen adsorbed on the photocatalyst (TiO_2). The photocatalytic properties of TiO_2 films for the degradation of MO process under UV irradiation (λ=365 nm) and +1.5 V applied potential are illustrated in Fig.7. As can be seen from Fig.7, at t=0 min, the absorption peaks of MO reaches the maximal value at 465 nm then after 10 min decreases rapidly and completely decolorizes of MO within different times in the presence TiO_2 film. Moreover, MO degradation was faster for films synthesize via PE mode than synthesize via DE. This could be attributed to the size of TiO_2 films. is apparent form Fig.7 that after 360 min, the MO degradation was faster on the TiO_2 film synthesis at T_{off}=1 s compared than synthesis at T_{off} =2 s and 3 s. This is due to the increase of production rate of oxygen species such as, $^{\bullet}O^{-2}$ and $^{\bullet}OH$, which affected the degradation of MO. We were also interested in influence of chosen process parameters to MO photodegradation rate. One of these parameters was the mode of synthesis DE and PE.

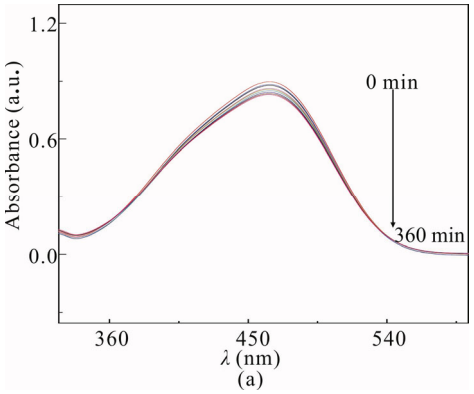

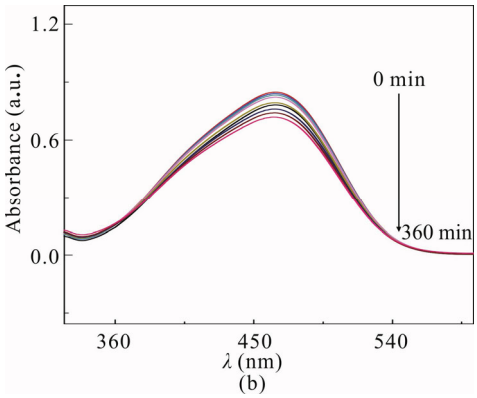

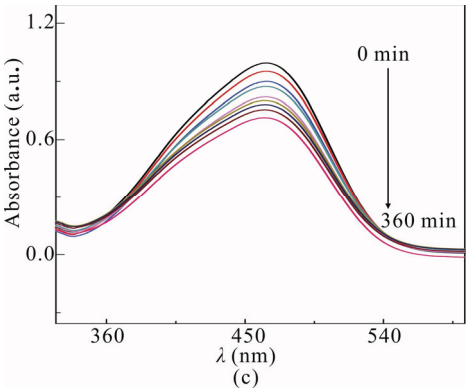

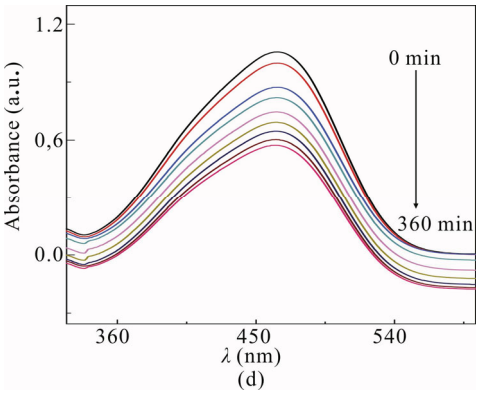

Fig.7 The series of absorption spectra of MO under UV irradiation (λ=365 nm) and fixed potential of +1.5 V, in presence of TiO_2 synthesized by (a) DE and PE at different T_{off}: (b) T_{off}=3 s, (c) T_{off} =2 s, and (d) T_{off} =1 s

In Fig.8(a), we have presented the photoelectrocatalytic degradation of MO for TiO_2 thin films, obtained by DE and PE at different time-off, under UV irradiation. As first remark, the degradation rate of MO for the film obtained by DE mode was very low compared to the other mode. In addition, it seen clear that the degradation rate of MO is reduced with decreasing time-off duration of TiO_2 catalyst, which showing that the photonic efficiency was higher for TiO_2 synthesized at low time-Off duration[45]. For further investigation on the features of photoelectrocatalytic degradation rate was achieved from the plot of the concentration of MO versus illumination time up to 360 min, witnessed in Fig.8(b). The initial concentrations of MO (C_0) the photocatalytic degradation rate of organic compounds can be explained by a pseudo-first order reaction, with the following Eq.(7) demonstrating the relationship of C and t[46]

$$\ln\frac{C}{C_K}=Kt\,, \tag{7}$$

where K is the rate constant of the photoelectrocatalytic degradation, t is the irradiation time, C_0 is the initial concentration of MO and C is the concentration of MO at time t. After calculation, It is found that the rate constant of the photoelectron-catalytic degradation as follow: 0.000 2 (DE), 0.000 6, 0.000 8, and 0.001 min^{-1} for 3 s, 2 s, and 1 s T_{off} duration, respectively. The similar observation was found by Lakhdari et al[45] in the case of ZnO

films synthesised via PE mode. The increasing of rate constant can be explained by type of defect and oxygen defect concentration[47].

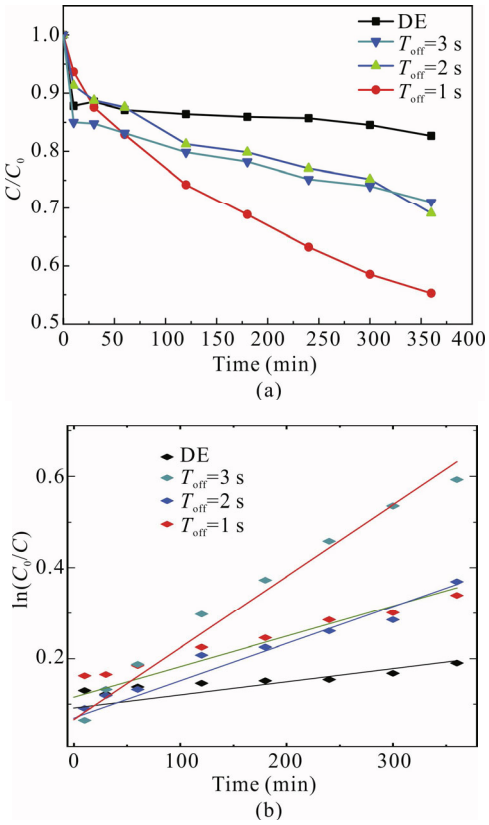

Fig.8 (a) Photoelectrodegradation of MO for 360 min in presence of TiO_2 deposited by DE and PE at different T_{off} under UV irradiation (λ=365 nm) and fixed potential of +1.5 V; (b) The photoelectrocatalytic degradation rate of MO by TiO_2 films deposited by DE and PE at different T_{off}

Fig.9 reveals the degradation percentage of MO for TiO_2 films, deposited at DE end PE in different T_{off}, under UV irradiation. The efficiency of the degradation D(%) reaction was determined using Eq.(8)[45,48]

$$D(\%)=(C_0-C/C_0)\times 100, \quad (8)$$

where C_0 is the initial MO concentration at 0 min and C is the concentration at a time t. According to the Lambert-Beer law, after 360 min of degradation, a rate of 17.27% (DE), 28.65%, 31.19%, and 44.79% was obtained for T_{off} of 3 s, 2 s and 1 s, respectively. As seen, the TiO_2 films synthesized by PE mode indicate a photoelectrocatalytic efficiency higher to that of the TiO_2 films obtained by DE mode. The origin of this result can be explained by structure, morphology and photocurrent response of TiO_2 film.

To sum up, herein we report a comparative study of a DE and PE methods at three time-off duration (3 s, 2 s, and 1 s) of TiO_2 films and its effect on photoelectrocatalysis degradation of MO. The main results can be summarized as follows. The XRD data shows anatase phase

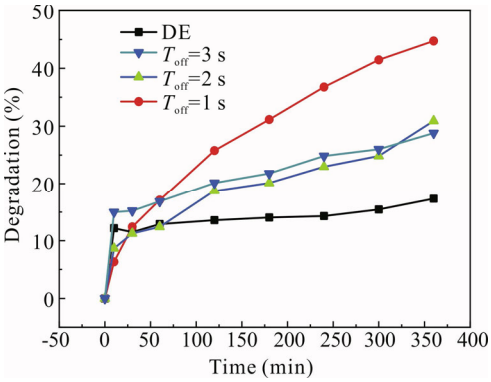

Fig.9 Degradation percentage versus irradiation time plot of MO degradation for TiO_2 deposited by DE and PE at different T_{off}

for all films with a strong intensity peak for (101) orientation for the film obtained by PE. The crystallite size increases with decreasing of T_{off} duration. However, the films synthesis by DE gives bigger crystallite size. All obtained films are relatively homogeneous and distributed almost uniform on the ITO substrate surface. The photocurrent response reveal n-type conductivity of TiO_2 thin films and show us the big difference between DE and PE mode (1.12 μA/cm^{-2} and 12.59 μA/cm^{-2}) respectively with a larger response at low T_{off}. Physicochemical analyses show that the properties and photo-activity of the obtained TiO_2 films are significantly affected by the DE, PE mode and time-off duration. The obtained results show that TiO_2 synthesis by PE mode improved photoelectrocatalysis properties that lead to faster MO degradation. Finally, this work assesses the feasibility of using TiO_2 thin films synthesis via PE mode at low T_{off} as photocatalytic degradation of MO.

References

[1] Scarpelli F., Mastropietro T., Poerio T. and Godbert N., Mesoporous TiO_2 Thin Films: State of the Art, Titanium Dioxide-Material for a Sustainable Environment, 57 (2018).

[2] Teferi B., Schnupf U., Manseki K., Sugiura T. and Vafaei S., Synthesis and Deposition of Rutile TiO_2 for Dye-Sensitized Solar Cell Applications, In ASME International Mechanical Engineering Congress and Exposition, American Society of Mechanical Engineers, V006T006A093 (2019).

[3] Zhang Y., Chen J., Hou G., Li D., Wu Y., Xu J., Xu L. and Chen K., Optics Express **28**, 6064 (2020).

[4] Woods R., Searle J., Pursglove A. and Worsley D., Journal of Environmental Chemical Engineering **7**, 103336 (2019).

[5] Rzaij J.M. and Abass A.M., Journal of Chemical Reviews **2**, 114 (2020).

[6] Nebatti A., Pflitsch C., Eckert C. and Atakan B., Progress in Organic Coatings **67**, 356 (2010).

[7] Fujishima A., Rao T.N. and Tryk D.A., Journal of Photochemistry and Photobiology C: Photochemistry Reviews **1**, 1 (2000).
[8] Hoffmann M.R., Martin S.T., Choi W. and Bahnemann D.W., Chemical Reviews **95**, 69 (1995).
[9] Cherrak R., Hadjel M., Benderdouche N., Adjdir M., Mokhtar A., Khaldi K., Sghier A. and Weidler P.G., Silicon **12**, 927 (2019).
[10] Tong H., Ouyang S., Bi Y., Umezawa N., Oshikiri M. and Ye J., Advanced Materials **24**, 229 (2012).
[11] Zhao W., Bai Z., Ren A., Guo B. and Wu C., Applied Surface Science **256**, 3493 (2010).
[12] Seong S.G., Kim E.J., Kim Y.S., Lee K.E. and Hahn S.H., Applied Surface Science **256**, 1 (2009).
[13] Haider A.J., AL-Anbari R.H., Kadhim G.R. and Salame C.T., Energy Procedia **119**, 332 (2017).
[14] Li J.-G., Ikeda M., Tang C., Moriyoshi Y., Hamanaka H. and Ishigaki T., The Journal of Physical Chemistry C **111**, 18018 (2007).
[15] Di Paola A., Bellardita M. and Palmisano L., Catalysts **3**, 36 (2013).
[16] Rasheed M. and Barillé R., Journal of Non-Crystalline Solids **476**, 1 (2017).
[17] Abou-Helal M. and Seeber W., Applied Surface Science **195**, 53 (2002).
[18] Chen Z., Dündar I., Acik I.O. and Mere A., In IOP Conference Series: Materials Science and Engineering **503**, 012006 (2019).
[19] Shinde V., Gujar T. and Lokhande C., Sensors and Actuators B: Chemical **120**, 551 (2007).
[20] Meng L., Wang Z., Yang L., Ren W., Liu W., Zhang Z., Yang T. and Dos Santos M., Applied Surface Science **474**, 211 (2019).
[21] Safranek W.H., The Properties of Electrodeposited Metals and Alloys: a Handbook, American Electroplaters and Surface Finishers Society, 1986.
[22] Aliofkhazraei M. and Makhlouf A.S.H., Hand-book of Nanoelectrochemistry: Electrochemical Synthesis Methods, Properties, and Characteriz-ation Techniques, Springer, 2016.
[23] El Moursli F.C., Douayar A., Hajji F., Nouneh K., Guessous A., Nabih K., Hadri A. and Abd-Lefdil M., Sensors & Transducers **27**, 137 (2014).
[24] Wang H., Song Y., Liu W., Yao S. and Zhang W., Materials Letters **93**, 319 (2013).
[25] Gal D., Hodes G., Lincot D. and Schock H.-W., Thin Solid Films **361**, 79 (2000).
[26] Khan R., Hassan M.S., Jang L.-W., Yun J.H., Ahn H.-K., Khil M.-S. and Lee I.-H., Ceramics International **40**, 14827 (2014).
[27] Lajevardi S. and Shahrabi T., Applied Surface Science **256**, 6775 (2010).
[28] Wu M.-S., Ceng Z.-Z. and Chen C.-Y., Electro-chimica Acta **191**, 256 (2016).
[29] Gyftou P., Pavlatou E. and Spyrellis N., Applied Surface Science **254**, 5910 (2008).
[30] An H.-J., Jang S.-R., Vittal R., Lee J. and Kim K.-J., Electrochimica Acta **50**, 2713 (2005).
[31] Hosono E., Fujihara S., Kakiuchi K. and Imai H., Journal of the American Chemical Society **126**, 7790 (2004).
[32] Alexander L. and Klug H.P., Journal of Applied Physics **21**, 137 (1950).
[33] Thompson C.V., Annual Review of Materials Science **30**, 159 (2000).
[34] Najim J. and Rozaiq J., International Letters of Chemistry, Physics and Astronomy **10**, 137 (2013).
[35] Sarkar A., Ghosh S., Chaudhuri S. and Pal A., Thin Solid Films **204**, 255 (1991).
[36] Chakraborty P., Datta G. and Ghatak K., Physica B: Condensed Matter **339**, 198 (2003).
[37] Samanta P., Saha A. and Kamilya T., Chemical Synthesis and Optical Properties of ZnO Nanoparticles, Журнал нано-та електронної фізики, 04015-04011-04015-04012, 2014.
[38] Juma A.O., Acik I.O., Mikli V., Mere A. and Krunks M., Thin Solid Films **594**, 287 (2015).
[39] Ghosh S. and Basu R.N., Nanoscale Characterization, In Noble Metal-Metal Oxide Hybrid Nanoparticles, Elsevier, 65 (2019).
[40] Fathy N. and Ichimura M., Journal of Crystal Growth **294**, 191 (2006).
[41] Frade T., Lobato K., Carreira J.F., Rodrigues J., Monteiro T. and Gomes A., Materials & Design **110**, 18 (2016).
[42] Nezamzadeh-Ejhieh A. and Moazzeni N., Journal of Industrial and Engineering Chemistry **19**, 1433 (2013).
[43] Lee K.M., Lai C.W., Ngai K.S. and Juan J.C., Water Research **88**, 428 (2016).
[44] Kou J., Lu C., Wang J., Chen Y., Xu Z. and Varma R.S., Chemical Reviews **117**, 1445 (2017).
[45] Lakhdari M. and Habelhames F., Journal of Materials Science: Materials in Electronics **30**, 6107 (2019).
[46] Ahmed S., Rasul M., Brown R. and Hashib M., Journal of Environmental Management **92**, 311 (2011).
[47] Leelavathi A., Madras G. and Ravishankar N., Physical Chemistry Chemical Physics **15**, 10795 (2013).
[48] Lakhdari M., Habelhames F., Nessark B., Girtan M., Derbal-Habak H., Bonnassieux Y., Tondelier D. and Nunzi J.M., The European Physical Journal Applied Physics **84**, 30102 (2018).